KfK 5160
September 1993

Numerical Simulation of Liquid - Metal Flows in Radial - Toroidal - Radial Bends

S. Molokov, L. Bühler
Institut für Angewandte Thermo- und Fluiddynamik
Projekt Kernfusion

Kernforschungszentrum Karlsruhe

Kernforschungszentrum Karlsruhe
Institut für Angewandte Thermo– und Fluiddynamik
Projekt Kernfusion

KfK 5160

Numerical Simulation of Liquid – Metal Flows in Radial – Toroidal – Radial Bends

S. Molokov and L. Bühler

Kernforschungszentrum Karlsruhe GmbH, Karlsruhe

Kernforschungszentrum Karlsruhe GmbH
Postfach 3640, 76021 Karlsruhe

ISSN 0303-4003

Numerical Simulation of Liquid – Metal Flows in Radial – Toroidal – Radial Bends

Abstract

Magnetohydrodynamic flows in a U–bend and right–angle bend are considered with reference to the radial–toroidal–radial concept of a self–cooled liquid–metal blanket. The ducts composing bends have rectangular cross–section. The applied magnetic field is aligned with the toroidal duct and perpendicular to the radial ones. At high Hartmann number the flow region is divided into cores and boundary layers of different types. The magnetohydrodynamic equations are reduced to a system of partial differential equations governing wall electric potentials and the core pressure. The system is solved numerically by two different methods. The first method is iterative with iteration between wall potential and the core pressure. The second method is a general one for the solution of the core flow equations in curvilinear coordinates generated by channel geometry and magnetic field orientation. In the present report a detailed description of the methods is given. Results obtained by the two methods are in good agreement. Both methods show, that the 3D -pressure drop of MHD flows in a U -bend is not a critical issue for blanket applications.

Numerische Simulation von Flüssigmetall – Strömungen in Radial – Toroidal – Radial Krümmern

Zusammenfassung

Gegenstand dieses Berichts sind magnetohydrodynamische Strömungen in einer U–Umlenkung und in einer rechtwinkligen Umlenkung, als Elemente eines selbstgekühlten radial-toroidal-radialen Flüssigmetall-Blankets. Das angelegte Magnetfeld zeigt in Richtung des toroidalen Kanals und steht senkrecht zur radialen Richtung. Für große Hartmann-Zahlen teilt sich das Strömungsgebiet in Kernströmungsbereiche (Cores) und in Grenzschichten. Die magnetohydrodynamischen Gleichungen lassen sich zu einem System von partiellen Differentialgleichungen zur Bestimmung des elektrischen Potentials der Kanalwand und des Core-Drucks vereinfachen. Dieses System wird mit zwei verschiedenen Verfahren numerisch gelöst. Bei der ersten Methode handelt es sich um ein iteratives Verfahren mit Iterationen zwischen den Werten des Wandpotentials und des Core-Drucks. Das zweite Verfahren ist ein allgemeines Verfahren zur Lösung der Kernströmungsgleichungen in gekrümmten Koordinaten, die durch die Kanalgeometrie und durch die Orientierung des Magnetfeldes vorgegeben werden. Dieser Bericht gibt eine Beschreibung beider Verfahren. Die Ergebnisse, die mit beiden Methoden gewonnen wurden, stimmen gut überein. Beide Methoden zeigen, daß 3D-Druckverluste von MHD Strömungen in einer U-Umlenkung für Blanket- Anwendungen unkritisch sind.

Numerical Simulation of Liquid – Metal Flows in Radial – Toroidal – Radial Ducts

Contents

1 Introduction

Magnetohydrodynamic (MHD) flows play an important role in liquid metal cooled fusion reactor blankets. Since an electrically conducting fluid has to flow through regions of the plasma confining strong magnetic field, currents are induced within the fluid. They close their loop in thin boundary layers or in electrically conducting channel walls and create considerably high pressure drop and a quite different flow structure compared to ordinary hydrodynamic (OHD) flows.

In several blanket designs effort has been made to achieve high velocities for an effective heat transfer in the plasma facing first wall coolant channels. It is proposed to reduce MHD pressure drop by choosing the flow direction aligned with the main toroidal component of the magnetic field. Toroidal channels are fed by larger poloidal ones (Smith *et al.* 1985) or as in the Radial– Toroidal– Radial (RTR)– concept (Malang *et al.* 1988) by radial channels. In these channels, where the flow suffers from strong MHD interaction, the fluid flows over a short distance. Both designs of liquid metal blankets involve MHD flows in straight ducts where the magnetic field is nearly perpendicular to the mean flow direction or nearly OHD flow in ducts aligned with the magnetic field, far away from the region where 3–D effects are important.

The MHD flow exhibits the core and boundary layers as the ratio of electromagnetic to viscous force given by the square of the Hartmann number $M = B_0 L(\sigma/\rho\nu)^{\frac{1}{2}}$ is large. Here B_0 is the applied constant magnetic field, L is a characteristic dimension of the cross section and σ, ρ, ν are electrical conductivity, density and kinematic viscosity of the fluid. In fully developed MHD flows in rectangular ducts two main types of boundary layers occur. The first type, which is called the Hartmann layer, appears at walls perpendicular to magnetic field lines. Its thickness is $O(M^{-1})$. The Hartmann layer matches the core of the fluid, where viscous effects are negligible, to conditions at walls. The flow in the Hartmann layer is governed by a system of ordinary differential equations. If the magnetic field is tangential to a channel wall, referred by many authors as a side wall, the second type of boundary layer appears at a side wall with dimensionless thickness $O(M^{-\frac{1}{2}})$. The flow in the layer is governed by a system of diffusion equations, and therefore this layer is called parabolic. At large M this layer can carry an $O(1)$ volume flux since high fluid velocities $O(M^{\frac{1}{2}})$ are possible inside. If there is no component of the magnetic field perpendicular to duct walls, i.e. the magnetic field is aligned with the flow, MHD is reduced to OHD with velocity profiles of Poiseuille type for fully developed flows.

According to the RTR concept we call the ducts with axes perpendicular to the magnetic field the radial ducts, whereas ducts aligned with the field are called the toroidal ducts. Radial and toroidal ducts are connected by bends which may cause considerable 3–D effects on pressure drop and velocity distribution. The geometry of a symmetric radial – toroidal – radial U–bend which is treated in this paper, is shown in figure 1.1. The characteristic length L is half the distance between the side walls. This geometry includes two limiting cases, namely a 90^o bend, if the length of toroidal duct is infinite ($l \longrightarrow \infty$) and the 180^o bend, if the toroidal duct length reaches its smallest value $l=a$. The magnetic field may be perfectly aligned with the toroidal direction $\hat{y}$ or slightly turned in the $x0y$ plane by the angle of α. Bends with positive or negative inclination are called forward or backward elbows, respectively.

3-D effects which are critical issues for any toroidal concept were estimated in the past by Hunt & Holroyd (1977) and Holroyd (1980), or analyzed recently in detail by Moon & Walker (1990), Moon, Hua & Walker (1990) or Hua & Walker (1991) for a 90^o bend with non – perfectly aligned toroidal duct ($\alpha \neq 0^o$). All referred works are based on the assumption, that the magnetic field is constant and not affected by the flow (small magnetic Reynolds number). It has also been supposed, that inertial effects, which are always present in real 3-D flows, had negligible influence on the flow structure, since the ratio of electromagnetic force to inertial force is assumed to be sufficiently large. If v_0 is a characteristic velocity, this ratio is determined by the interaction parameter $N = \sigma L B_0^2/\rho v_0$. Inertial effects can be neglected if $N >> M^{3/2}$ (Hunt & Leibovich 1967). The present report treats the flow in a U-bend and in a 90^o bend for $\alpha=0^o$. This case has not been covered in any of the cited papers. The assumptions are the same as in the above mentioned papers. The equations governing the flow are reduced to the core flow equations. The latter are solved by the two different methods. The aim of the present report is to present descriptions of both methods and comparison of results. The detailed flow analysis is given by Molokov & Bühler (1993).

Figure 1.1 a) Geometry of the U-bend; b,c) flow subregions

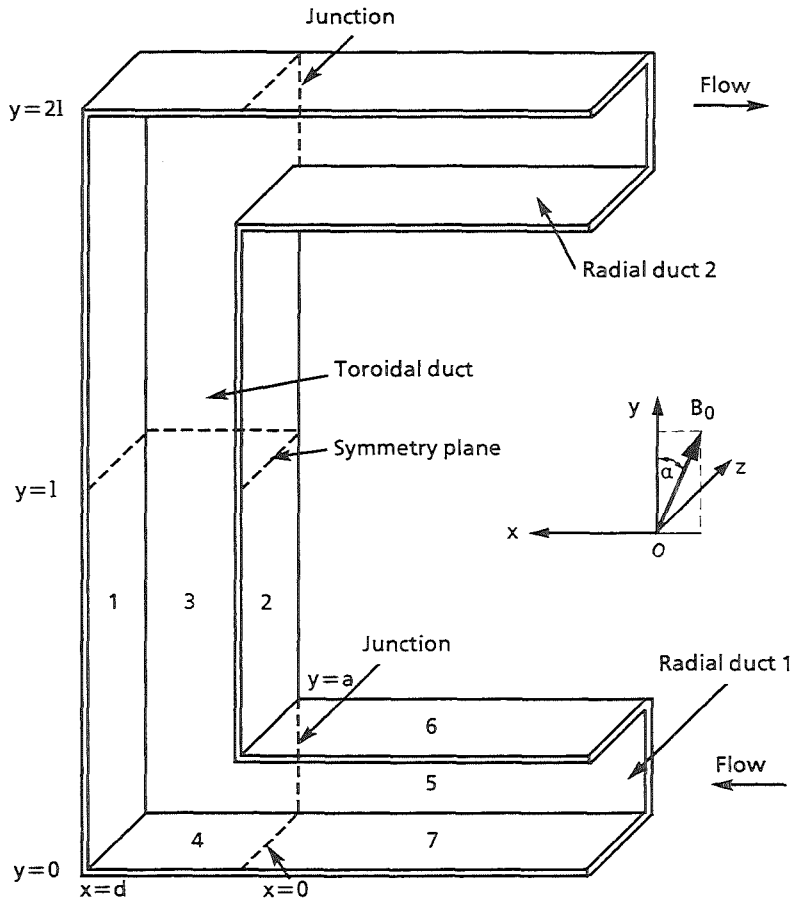

Fig. 1.1a

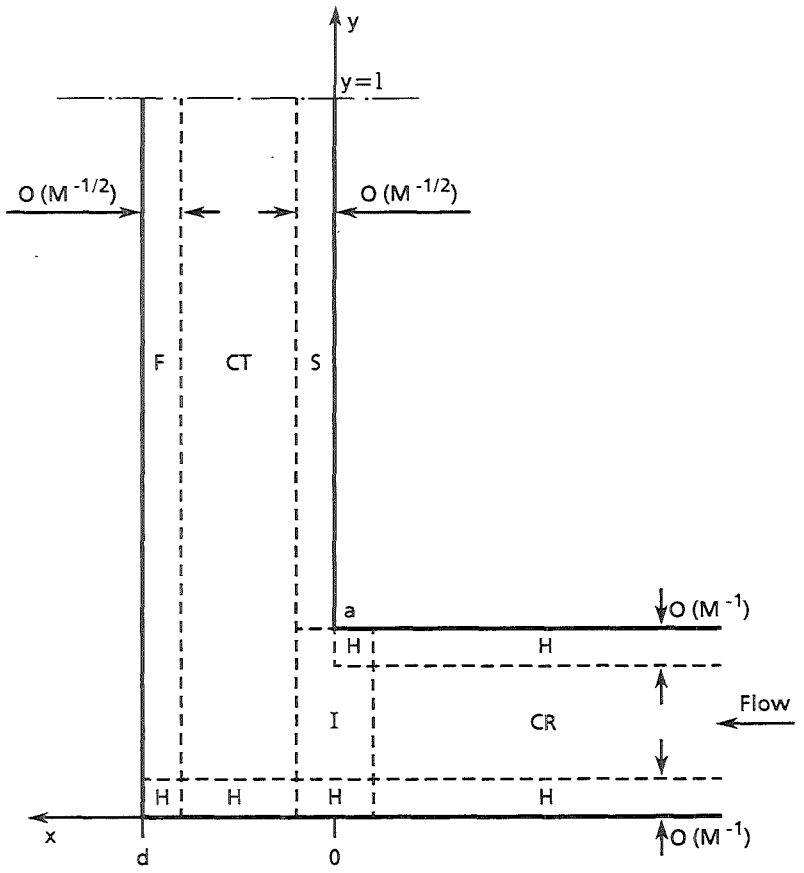

Fig. 1.1b

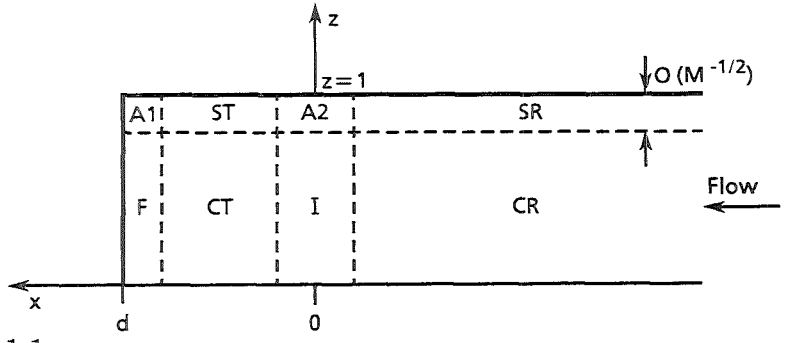

Fig. 1.1c

2. Formulation

Consider the steady flow of a viscous conducting incompressible fluid in a U–bend (figure 1.1a). The U–bend consists of three parts:

– radial duct 1 at $x \le 0,\ -1 \le z \le 1,\ 0 \le y \le a$;

– radial duct 2 at $x \le 0,\ -1 \le z \le 1,\ 2l-a \le y \le 2l$;

– toroidal duct at $0 \le x \le d,\ -1 \le z \le 1,\ 0 \le y \le 2l$.

All ducts have rectangular cross–section.

A strong uniform external magnetic field $\underline{B} = B_0\,\hat{y}$ ($\alpha=0^o$)is aligned with four walls of the toroidal duct, namely, $z=\pm 1$, $x=0$, and $x=d$. The U–bend is supposed to be symmetric with respect to both $y=l$ and $z=0$ planes, and since inertial effects are neglected, the flow in the quarter of the duct $y \le l$, $z \ge 0$ is considered under appropriate symmetry conditions. The walls of this part of the bend are numbered from 1 to 7, as shown in figure 1.1a.

The dimensionless inertialess inductionless equations governing the problem are (e.g. Moon & Walker 1990)

$$M^{-2}\nabla^2 \underline{v} + \underline{j}\times\hat{y} = \nabla p, \qquad (1a)$$

$$\underline{j} = -\nabla\phi + \underline{v}\times\hat{y}, \qquad (1b)$$

$$\nabla\cdot\underline{v} = 0, \qquad (1c)$$

$$\nabla\cdot\underline{j} = 0, \qquad (1d)$$

where the fluid velocity $\underline{v} = u\hat{x} + v\hat{y} + w\hat{z}$, the electric current density $\underline{j}$, the electric potential ϕ and the pressure p are normalized by v_0 (the average fluid velocity at a cross–section $x=const$ of the radial duct *1*), $\sigma v_0 B_0$, $v_0 B_0 L$ and $\sigma v_0 B_0^2 L$, respectively.

The boundary conditions at each wall are the non–slip condition

$$\underline{v} = 0 \qquad (1e)$$

and the thin–wall condition

$$\underline{j} \cdot \underline{n}_i = c_i \nabla_i^2 \phi_i, \qquad (1f)$$

where $\underline{n}_i$ is the normal unit vector to the wall i, into the fluid. ∇_i is the gradient in the plane of the wall; ϕ_i is the fluid potential on the wall i $(i=1, \ldots, 7)$. Since walls of the ducts are thin and electric potential is continuous across the fluid-wall interface wall potential is equal to ϕ_i as well. Once ϕ_i is known, the currents $\underline{j}_i$ in the wall i are determined from equation

$$\underline{j}_i = -\frac{\sigma_i}{\sigma} \nabla_i \phi_i. \qquad (2)$$

The symmetry conditions for pressure and electric potential are

$$\phi = p = 0 \text{ at } y = l, \qquad (1g,h)$$

$$\frac{\partial p}{\partial z} = \phi = 0 \text{ at } z = 0. \qquad (1i,j)$$

In the radial duct, far away from the junction, the flow is fully developed. This reflects in the conditions

$$\frac{\partial \phi}{\partial x} = \frac{\partial p}{\partial z} = \frac{\partial p}{\partial y} = 0 \text{ as } x \longrightarrow -\infty. \qquad (1k\text{–}m)$$

The symmetry conditions and the conditions at infinity for other flow variables are not used here. They can be derived from the conditions $(1i\text{-}m)$ and the governing equations.

The fluid velocity satisfies the constant volume–flux condition

$$\int_0^1 dz \int_0^a u\,dy = a \qquad (1n)$$

at cross–section $x=const$ of the radial duct and

$$\int_0^1 dz \int_0^d v\,dx = a \qquad (1o)$$

at cross–section y=*const* of the toroidal duct in the region $a \leq y \leq l$.

In section 2 an asymptotic solution (as $M \longrightarrow \infty$) to the problem *(1)* is constructed by means of matched asymptotics.

3. Solution by method 1

As $M \longrightarrow \infty$, the interior of the bend may be divided into certain subregions (figure 1.1b,c), where the flow is governed by the reduced equations. Most of the flow region is occupied by the inviscid cores *CR* in the radial duct *1* and *CT* in the toroidal duct. Cores of both ducts are separated from the walls and from each other by the layers of two types:

- the Hartmann layers *H* near the walls perpendicular to the magnetic field with a thickness of $O(M^{-1})$;
- the parabolic layers parallel to the magnetic field with $O(M^{-\frac{1}{2}})$ thickness.

The latter ones are at the side walls of both ducts (regions *SR* and *ST*), the first wall (region *F*), the second wall (region *S*), and inside the fluid at the junction $x=0$ (internal layer, region *I*). At $y=a$ layers *I* and *S* merge, and therefore they must be treated simultaneously.

Near the corners $z=1$, $x=d$ and $z=1$, $x=0$, where layers *ST* and *SR* intersect with layers *F*, *S*, and *I*, layers *A1* and *A2* are formed with x- and z- dimensions both of $O(M^{-\frac{1}{2}})$. The flow in the layers *A1* and *A2* is governed by a system of two–dimensional diffusion equations, and therefore they may be called two–dimensional parabolic layers. Similar to the core regions, parabolic layers are separated from the walls perpendicular to the field by the Hartmann layers.

In the core regions viscous terms in the equation *(1a)* may be neglected. This corresponds to the limit $M \longrightarrow \infty$. The general solution of the resulting equations is (e.g. Moon & Walker 1990)

$$u_c = \frac{\partial \phi_c}{\partial z} - \frac{\partial p_c}{\partial x}\,, \tag{3a}$$

$$v_c = y\left[\frac{\partial^2 p_c}{\partial x^2} + \frac{\partial^2 p_c}{\partial z^2}\right] + g_1\,, \tag{3b}$$

$$w_c = -\frac{\partial \phi_c}{\partial x} - \frac{\partial p_c}{\partial z}\,, \tag{3c}$$

$$j_{xc} = \frac{\partial p_c}{\partial z}\,, \qquad j_{yc} = -\frac{\partial \phi_c}{\partial y}\,, \qquad j_{zc} = -\frac{\partial p_c}{\partial x}\,, \tag{3d-f}$$

$$\phi_c = g_2 + g_3 y \tag{3g}$$

here $p_c(x,z)$ is the core pressure; $g_n(x,z)$ $(n=1\text{-}3)$ are integration functions. Throughout this paper subscripts of flow variables denote the flow subregion, where corresponding limit equations are valid. Subscript c denotes both CT and CR.

The jumps in the component of electric current normal to the wall across the Hartmann layers and parabolic layers are at most $O(M^{-1})$ and $O(M^{-\frac{1}{2}})$, respectively. The jump of the core potential across the Hartmann layers is at most $O(M^{-2})$. Neglecting these jumps has the following consequences:

– normal component of core velocity vanishes at the tops and the bottoms of both ducts, i.e.

$$v_{CR} = 0 \text{ at } y=0 \text{ and at } y=a,\ x\lesssim 0; \tag{4a}$$

$$v_{CT} = 0 \text{ at } y=0,\ x\gtrsim 0; \tag{4b}$$

– core current satisfies the thin–wall conditions $(1f)$ at all walls, i.e.

$$\underline{j}_c \cdot \underline{n}_i = c_i \nabla_i^2 \phi_i \text{ at wall } i\ (i=1,..,7); \tag{4c}$$

– core potentials, estimated on walls $4, 6,$ and 7 are equal to potentials of these walls, i.e.

$$\phi_c = \phi_i \text{ at wall } i\ (i=4,6,7). \tag{4d}$$

3.1 Core of the radial duct

Substituting expressions (3) into the equations $(4a\text{-}d)$ determines the unknown functions g_n to give the expressions for the core–flow variables in the radial duct in terms of wall potentials and core pressure, namely

$$u_{CR} = -\frac{\partial p_{CR}}{\partial x} + \left(1 - \frac{y}{a}\right)\frac{\partial \phi_7}{\partial z} + \frac{y}{a}\frac{\partial \phi_6}{\partial z}, \tag{5a}$$

$$v_{CR} = 0, \tag{5b}$$

$$w_{CR} = -\frac{\partial p_{CR}}{\partial z} + \left(\frac{y}{a} - 1\right)\frac{\partial \phi_7}{\partial x} - \frac{y}{a}\frac{\partial \phi_6}{\partial x}, \tag{5c}$$

$$\phi_{CR} = \phi_6 + (1 - \frac{y}{a})(\phi_7 - \phi_6) \ , \qquad (5d)$$

$$j_{xCR} = \frac{\partial p_{CR}}{\partial z} \ , \qquad j_{yCR} = a^{-1}(\phi_7 - \phi_6), \qquad j_{zCR} = - \frac{\partial p_{CR}}{\partial x} \ , \qquad (5e\text{-}g)$$

and provides the equations

$$c_5 \nabla_5^{\,2} \phi_5 = \frac{\partial p_{CR}}{\partial x}(x, z=1) \ , \qquad (6a)$$

$$c_7 \nabla_7^{\,2} \phi_7 = a^{-1}(\phi_7 - \phi_6) \ , \qquad (6b)$$

$$c_6 \nabla_6^{\,2} \phi_6 = - a^{-1}(\phi_7 - \phi_6) \ , \qquad (6c)$$

$$\frac{\partial^2 p_{CR}}{\partial x^2} + \frac{\partial^2 p_{CR}}{\partial z^2} = 0 \ . \qquad (6d)$$

In the radial duct *1* the volume flux in the x-direction is carried by the core CR and the side layer SR, so that it is a sum of volume fluxes q_{CR} and q_{SR}, which read

$$q_{CR,x} = -a \int_0^1 \frac{\partial p_{CR}}{\partial x} dz + \frac{a}{2}\Big[\phi_6(x, z=1) + \phi_7(x, z=1)\Big] \ ; \qquad (7a)$$

$$q_{SR,x} = \int_0^a \phi_5(x, y)\, dy - \frac{a}{2}\Big[\phi_6(x, z=1) + \phi_7(x, z=1)\Big] \ . \qquad (7b)$$

The expression *(7b)* is obtained by the integration of the z-component of the Ohm's law across the layer SR (e.g. Moon & Walker 1990). Substituting *(7a)* and *(7b)* into the equation *(1n)* gives the condition

$$\int_0^a \phi_5(x, y)\, dy - a \int_0^1 \frac{\partial p_{CR}}{\partial x}(x, z)\, dz = a. \qquad (6e)$$

3.2 Core of the toroidal duct

Substituting the equations *(3)* into the equations *(4b-d)* and the symmetry conditions *(1g,h)* gives the equations governing the wall potentials of the toroidal duct, namely

$$\nabla_1^2\phi_1 = \nabla_2^2\phi_2 = \nabla_3^2\phi_3 = 0, \quad lc_4\nabla_4^2\phi_4 = \phi_4. \tag{8a-d}$$

The core variables are expressed in terms of wall potentials as follows:

$$\phi_{CT} = (1 - \frac{y}{l})\phi_4, \qquad p_{CT} = 0; \tag{9a,b}$$

$$u_{CT} = \frac{\partial\phi_{CT}}{\partial z} = (1 - \frac{y}{l})\frac{\partial\phi_4}{\partial z}; \tag{9c}$$

$$v_{CT} = 0; \tag{9d}$$

$$w_{CT} = -\frac{\partial\phi_{CT}}{\partial x} = -(1 - \frac{y}{l})\frac{\partial\phi_4}{\partial x}; \tag{9e}$$

$$j_{xCT} = 0, \qquad j_{yCT} = \frac{1}{l}\phi_4, \qquad j_{zCT} = 0. \tag{9f-h}$$

Consider now the boundary conditions for the equations *(6)* and *(8)*. If walls i and k have a common boundary Γ_{ik}, continuity of the potential and the normal component of current density requires that

$$\phi_i = \phi_k, \quad c_i\frac{\partial\phi_i}{\partial\underline{s}_i} = -c_k\frac{\partial\phi_k}{\partial\underline{s}_k} \text{ at } \Gamma_{ik}, \tag{10a,b}$$

where $\underline{s}_i, \underline{s}_k$ are outward normal vectors to Γ_{ik} in the planes of the walls i and k, respectively.

Conditions *(1k, l)* of fully developed flow at infinity in the radial duct *1* give

$$\frac{\partial\phi_5}{\partial x} = \frac{\partial\phi_6}{\partial x} = \frac{\partial\phi_7}{\partial x} = \frac{\partial p_{CR}}{\partial z} = 0. \tag{10c-f}$$

Condition *(1m)* is satisfied by the function p_{CR} automatically.

The symmetry conditions *(1g-j)* give

$$\frac{\partial p_{CR}}{\partial z} = \phi_1 = \phi_2 = \phi_4 = \phi_6 = \phi_7 = 0 \ at \ z=0 \ , \qquad (10g-l)$$

$$\phi_1 = \phi_2 = \phi_3 = 0 \ at \ y=l \ . \qquad (10m-o)$$

The system of equations *(6)* and *(8)*, subject to the conditions *(10)* is solved numerically. After the solution is obtained, the flow in the core is reconstructed using the expressions *(5)* and *(9)*. The condition *(1o)* has not been used for derivation of the equations *(8)*.

3.3 Numerical algorithm

The systems of equations *(6)* and *(8)* are solved numerically. The numerical method is iterative with iterations between domains *1* to *7* and Eq. *6d* for the core pressure.

The boundary conditions are approximated as follows. If for the domain i potential at the boundary Γ_{ik} is given (Eq. *10a*), then for the domain k derivative of potentials is given, and vice versa. For approximating derivatives of potentials, underrelaxation is used in case of small ratio c_k/c_i.

For the pressure the boundary condition

$$\frac{\partial p}{\partial z} = \frac{1}{a}\int_0^a \frac{\partial \phi_5}{\partial x}\, dy \qquad at \ \ z=1$$

is used, which results from Eq. *(6e)*.

Since all equations are of Laplace and Helmholtz type on a rectangle, a fast Poisson solver has been used. Iterations were stopped when the differences in nodal pressures and wall potentials at two subsequent steps were less than 0.1 per cent.

4. Solution by method 2

4.1 The code

The other numerical calculation procedure applied to the radial–toroidal–radial U–bend problem is the core–flow code for calculating MHD–flows in general geometries and arbitrary magnetic fields. (Bühler 1993). The wall conductance ratio of channel walls should satisfy the relation $c >> M^{-\frac{1}{2}}$ if interior layers or side layers appear like in the considered flow problem. This assumption ensures that the conductivities of interior layers and side layers are unimportant for the flow outside these layers. However, if side layers appear and the above mentioned condition does not hold they are treated approximately by the code.

This code, which takes profit of characteristic MHD– properties along magnetic field lines, is designed for solving MHD-flow problems where the direction of the main flow is not aligned with the magnetic field lines. This fact requires some modifications of the standard code, since in toroidal duct all volume flux has to be carried exactly in the magnetic field direction. These modifications are outlined in the following chapters.

Flows in general geometries are calculated by means of a coordinate transformation. A transformation of the type

$$\underline{x} = \overline{\underline{x}}(u^1, u^2) + \underline{h}(u^1, u^2) \cdot u^3 \qquad (11a)$$

transforms every arbitrary channel geometry to a standard volume

$$0 \leq u^1, u^2 \leq 1 \; ; \; -1 \leq u^3 \leq 1 \; . \qquad (11b)$$

$\overline{\underline{x}}$ is an average surface and $\underline{h}$ is the half height of the channel cross section in $\underline{B}$- direction. Unfortunately, a transformation of this kind excludes walls, exactly parallel to magnetic field lines. For a treatment of flows in ducts with rectangular cross section (walls parallel to the $\underline{B}$- field are called side walls) these channels are approximated by channels with slightly elliptically deformed side walls. This approximation gives excellent results over a wide range of Hartmann– numbers or wall conduction ratios (Bühler 1993). The elliptical deformation of $\underline{B}$-field-parallel walls is used for side walls of radial ducts and also for side walls of toroidal duct. Walls *1* and *2* are chosen slightly deformed to avoid the same singular transformation problems. The whole geometry is shown in figure 4.1. Flow in this geometry approximates the flow of interest if the deformations ϵ_{sw}, ϵ_{2w} and ϵ_{1w} are

sufficiently small.

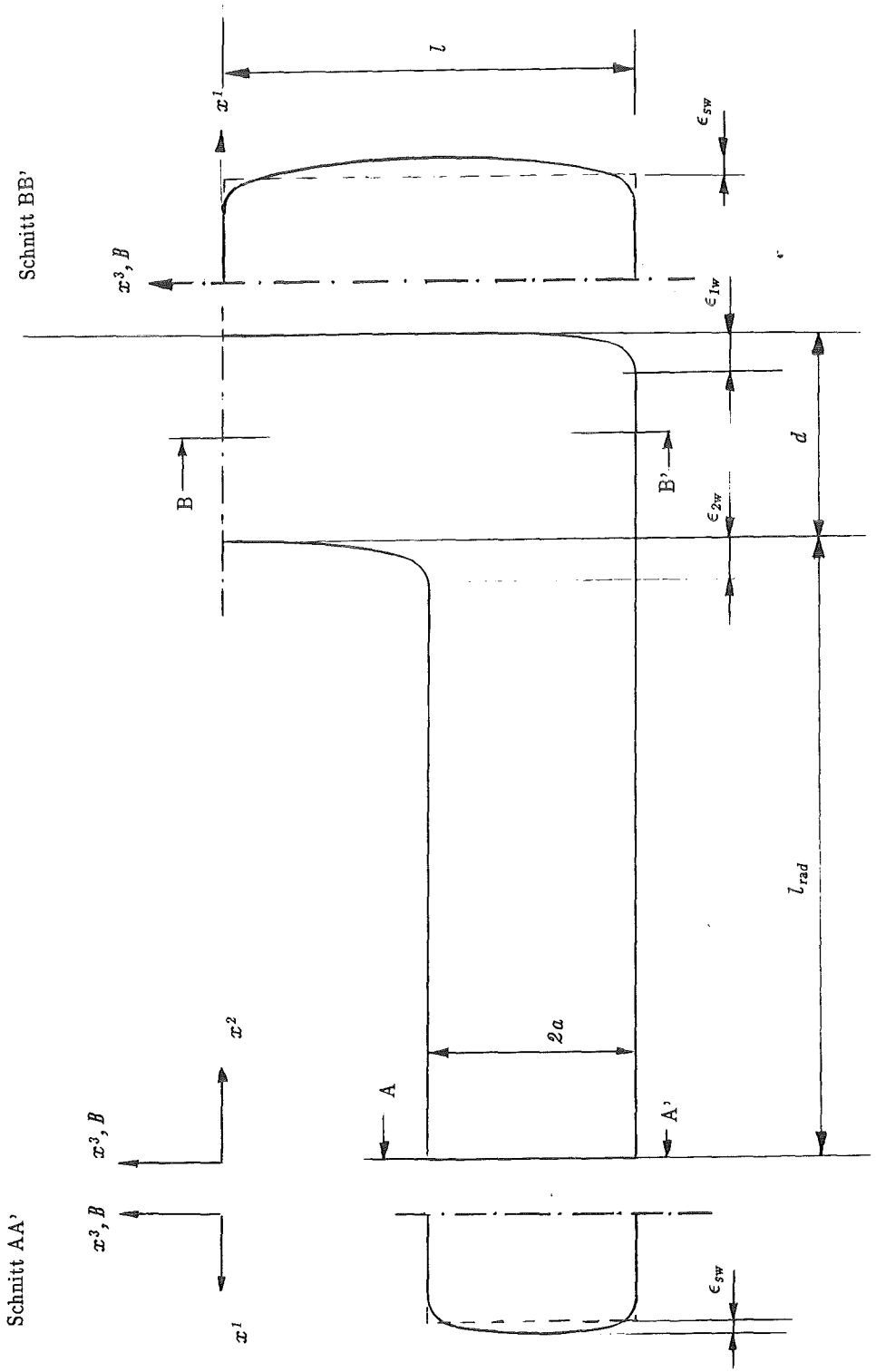

Figure 4.1 Geometry used by method 2. It approximates the real geometry if the elliptical deformations are small (ϵ_{sw}, ϵ_{2w}, $\epsilon_{1w} \longrightarrow \infty$)

As boundary condition for potential at solid walls the ***thin wall condition*** formulated in arbitrary non–orthogonal wall coordinates is used.

$$\underline{j} \cdot \underline{n} = -\sum_{i=1}^{2} \frac{\partial}{\partial x^i} \sum_{k=1}^{2} cA g_w^{ik} \frac{\partial \phi}{\partial x^k} \qquad (12)$$

c is the wall conductance ratio, which may be an arbitrary function of both independent coordinates $w^1=u^1$ and $w^2=u^2$ tangential to the walls $u^3=\pm 1$. The shape of the channel is represented by the contravariant components of the metric tensor $g_w{}^{ik}$ due to the use of a wall fitted coordinate system

$$\underline{x} = \underline{x}_w(w^1, w^2) + \underline{n}\, t(w^1, w^2) w^3 \qquad (11c)$$

with

$$0 \leq w^1, w^2 \leq 1; \; 0 \leq w^3 \leq 1 \; . \qquad (11d)$$

The coordinate w^3 in the wall normal direction $\underline{n}$ is eliminated from the equation of charge conservation in the wall by an integration in direction normal to the wall to give *(12)*. A represents the transformation of an area element of the wall fluid interface.

At the symmetry plane $x^3=0$ the potential is given by the symmetry condition

$$\phi = 0 \qquad (1g)$$

and has not to be calculated by by the using *(12)*.

After integration of the mass conservation equation the kinematic boundary conditions at all walls give the equation for calculating the core pressure $p(u^1, u^2)$. Along the symmetry plane $x^3=0$ pressure p is already defined by the symmetry condition

$$p = 0 \; . \qquad (1h)$$

An integration of the mass conservation equation with known pressure $p=0$ gives here the distribution of volume flux in the plane of symmetry.

The length of the radial duct l_{RAD} was chosen long enough that the conditions of fully developed flow

$$p = const, \frac{\partial \phi}{\partial x^2} = 0 \qquad (1k)$$

may be applied at $x^2=0$.

A more detailed description of this solution method, is given by Bühler (1993).

4.2 The grid

The used numerical grid is shown in figure 4.2. A non uniform grid spacing is used in the radial direction to resolve 3-D effects near the junction. The requirement of the numerical code to use a discretization with magnetic cross sections leads to an abrupt change in the step width in the region of $l_{RAD}-\epsilon_{2w}<x^2<l_{RAD}$. There is a jump between small steps at the top wall and larger steps at the second wall and between small steps and much smaller steps at at the side wall. This fact, and the strongly trapezoidal shape of wall elements near the junction can reduce the accuracy of the numerical solution, especially if the length of the toroidal channel is large. This may explain some discrepancy between results in table 1. If the flow is sensitive to small changes in wall potential (if c is small) this effect is more expressed. Nevertheless, results are in good agreement to such obtained by method 1, which is designed specifically to solve this problem. This can be checked in the table of comparison in the chapter 5.3.

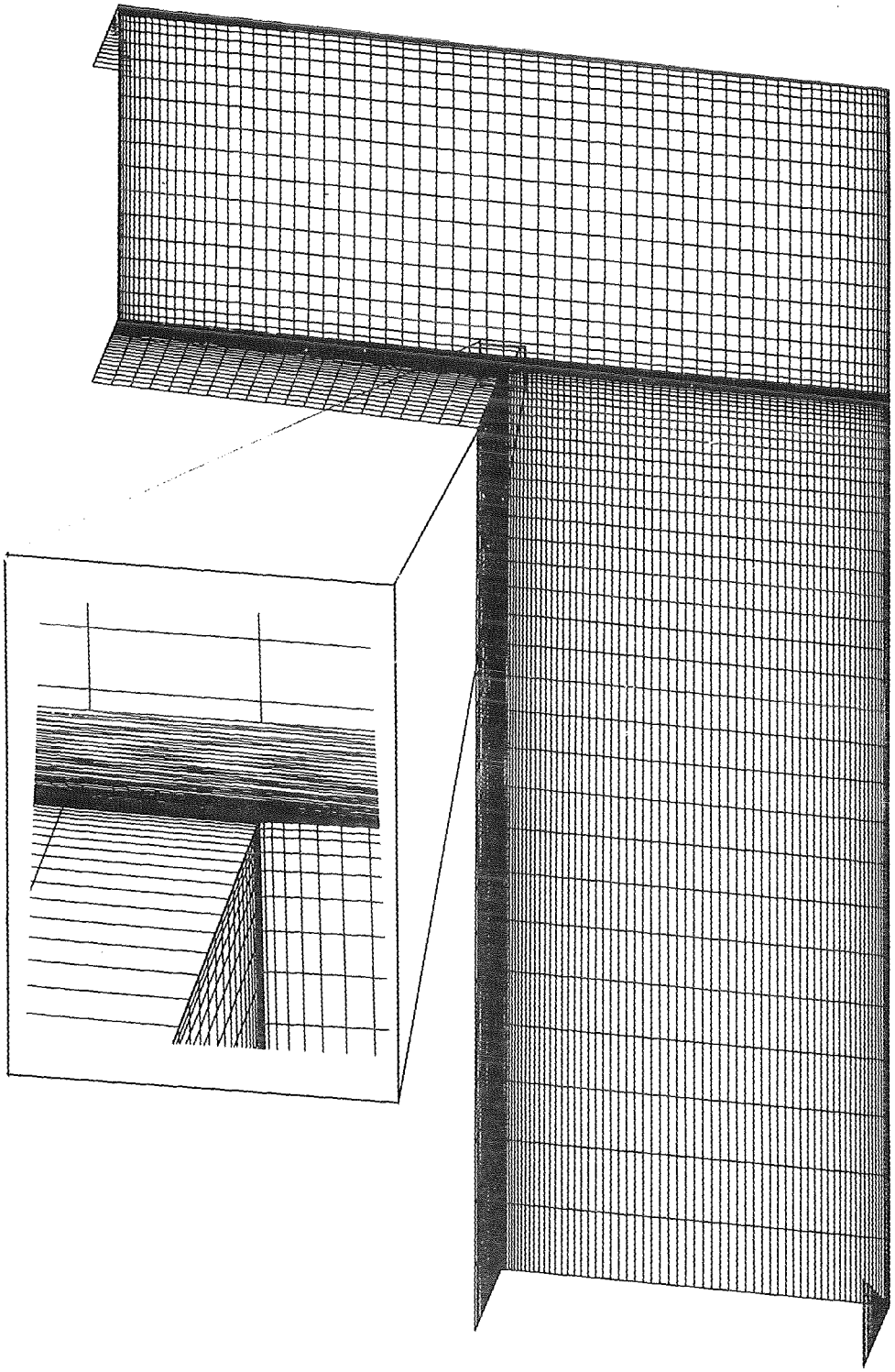

Figure 4.2 Used numerical grid

5. Results

5.1 Flow distribution in the radial duct

The flow structure in the radial duct does not show any unexpected behavior. Far away from the junction the flow exhibits the flat core and the high velocity side layers of a fully developed flow in a channel of thin conducting walls. If the fluid approaches the junction, velocity profile in the core is deformed. 3-D currents lead to a reduction of fluid velocity in the center of the duct, and to an increase of flow near the side walls. It is well known that this effect occurs in many three dimensional MHD flows (flows in variable fields, in expansions or contractions, or in bends). Figure 5.1 shows the x-component of the core velocity at several cross sections of the radial duct for parameters of the 'case 2c' (see table 5.1).

5.2 Flow distribution in the toroidal duct

Equations *(5b)* and *(9d)* indicate that in both cores the velocity component parallel to magnetic field lines is zero. For the toroidal duct this result means that the core does not carry volume flux in the main–flow direction and all volume flux is carried by high–velocity jets in the parabolic layers ST, F, I and S.

The total volume fluxes carried by layers F, ST, S and I in the y-direction at any cross section $y=const$ read (see Molokov & Bühler 1993)

$$q_{F,y} = \int_0^y \phi_1(y, z=1)\,dy = -\frac{1}{c_1} I_{1z}\,, \qquad (13)$$

$$q_{S,y} = a - \int_0^y \phi_3(x=0, y)\,dy \qquad (14)$$

$$q_{I,y} = -\,y \int_0^1 \frac{\partial p_{CR}}{\partial x}(x=0, z)\,dz \qquad (15)$$

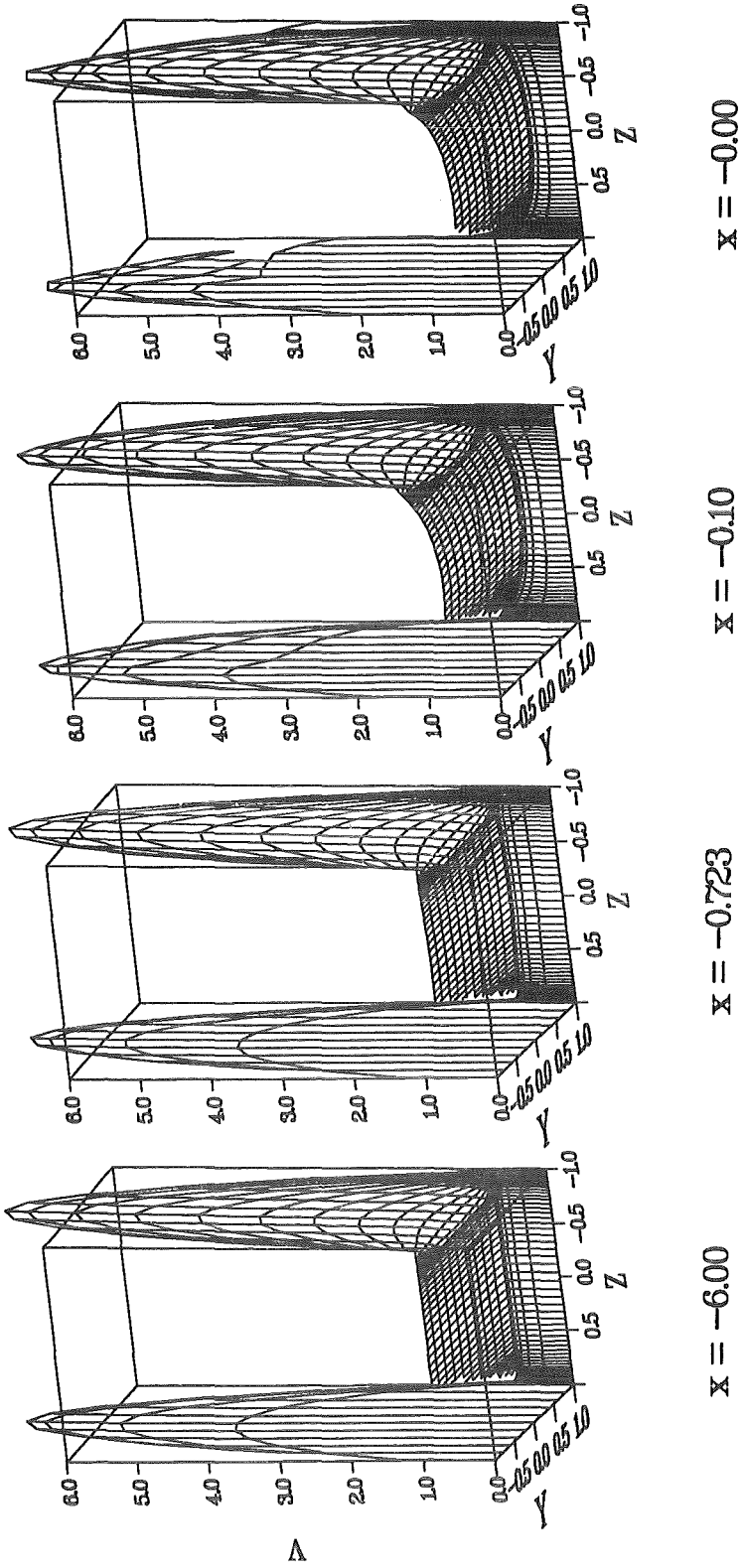

Figure 5.1 Velocity profiles in the radial duct

$$q_{ST,y} = \int_0^y \left[\phi_3(x=0,y) - \phi_3(x=d,y)\right] dy \qquad (16)$$

These flow rates give the most essential information about flow distribution in the toroidal duct.

5.3 Comparison between two methods

A comparison of results obtained by method 1 and method 2 is presented in table 5.1. The length of the considered radial duct is $l_{RAD}=6$.

Calculations by method 1 were done on a grid with 32 points per unit length in each direction.

A discretisation for the wall surface ($u^3 = \pm 1$) of 100×160 points in the radial direction (x^2-direction, $0 \leq u^2 \leq 1$) and along the channel wall of one half of a cross section (x^1-direction, $0 \leq x^1 \leq 1$), respectively, is used for calculations by method 2. The maximum residual error due to the direct solution method of the used solver for linear algebraic equations was smaller than 10^{-6}.

Table 5.1 Comparison of results for pressure drop Δp in a half of a U-bend ($y<l$) with a radial length of $l_{RAD} = 6.0$ and for flow rates in one half of the toroidal duct ($0<z<1$) at the symmetry plane $y=l$, obtained by the two different methods for several combinations of parameters.

	Parameter	$q_{F,y}$	$q_{ST,y}$	$q_{s,y}$	Δp	Method
1a	$c_T = \infty$			2.000	0.9690	1
	$c = 0.1$			2.000	0.9619	2
1b	$c_T = \infty$			2.000	2.0936	1
	$c = 0.5$			2.000	2.0946	2
2a	$c_F = \infty$ $c = 0.1$ $l = 2.0$		1.430	0.570	0.5338	1
			1.424	0.576	0.5445	2
2b	$c_F = \infty$ $c = 0.5$ $l = 2.0$		0.826	1.174	1.8889	1
			0.828	1.172	1.9147	2
2c	$c_F = \infty$ $c = 0.1$ $l = 4.0$		1.868	0.132	0.4931	1
			1.866	0.134	0.5159	2
2d	$c_F = \infty$ $c = 0.5$ $l = 4.0$		1.156	0.844	1.8273	1
			1.138	0.862	1.8613	2
3a	$c = 0.1$	0.108	1.354	0.538	0.5133	1
	$l = 2.0$	0.072	1.356	0.572	0.5447	2
3b	$c = 0.5$	0.082	0.754	1.164	1.8859	1
	$l = 2.0$	0.052	0.780	1.168	1.9029	2
3c	$c = 0.1$	0.390	1.490	0.120	0.4812	1
	$l = 4.0$	0.392	1.582	0.026	0.5228	2
3d	$c = 0.5$	0.270	0.930	0.800	1.8206	1
	$l = 4.0$	0.256	0.928	0.816	1.8726	2

6 Conclusions

The present analysis shows that 3–D pressure drop of MHD flows in U–bends and in right– angle bends is not a critical issue for applications in self– cooled liquid metal blankets. It is almost unimportant, compared to the 2–D pressure drop in the straight ducts perpendicular to the field (the radial ducts), which form one part of the bends. In this first part of the bend the flow exhibits the well known structures of 3–D MHD flows. Near the junction the fluid is pushed towards the side– regions and fluid velocity is deceased in the center of the duct and increased near the sides. In the other part of the bend (in the toroidal duct), however, the flow distribution is rather unexpected. The core of the toroidal duct does not carry any $O(1)$ volume flux. The total volume flux is confined to thin boundary layers along duct walls, which are aligned with the magnetic field and to the interior layer at the junction. A significant part of the total volume flux is carried along the first wall in a thin, high velocity layer if this wall is not a perfect conductor. This may lead to favorable heat transfer conditions.

Results were obtained by two completely different methods. The good agreement of results obtained by both methods validates both approaches and confirms the non trivial flow structure.

7 References

Bühler, L. 1993 Magnetohydrodynamische Strömungen flüssiger Metalle in allgemeinen dreidimensionalen Geometrien unter der Einwirkung starker, lokal variabler Magnetfelder. *KfK report* KfK5095.

Holroyd, R.J. 1980 An experimental study of the effects of wall conductivity, non–uniform magnetic fields and variable area ducts on liquid metal flows at high Hartmann number. Part 2. Ducts with conducting walls. *J. Fluid Mech.* **96**,355.

Hua, T.Q., Walker, J.S., Picologlou, B.F. & Reed, C.B. 1988 Three–dimensional magnetohydrodynamic flows in rectangular ducts of liquid–metal–cooled blankets. *Fusion Technology*, vol.14, 1389.

Hunt, J.C.R., Holroyd, R.J. 1977 Applications of laboratory and theoretical MHD duct flow studies in fusion reactor technology. *Culham Laboratory Report CLM–R169.*

Hunt, J.C.R., Leibovich, S. 1967 Magnetohydrodynamic flows in channels of variable cross – section with strong transverse magnetic field. *J. Fluid Mech.*, vol. 28, 241–260.

Malang, S., et. al. 1988 Self–cooled liquid–metal blanket concept, *Fusion Technolgy*, vol. 14, 1343.

Molokov, S. & Bühler, L. 1993 Liquid metal flow in a U-bend in a strong uniform magnetic field, *(submitted for publication).*

Moon, T.J. & Walker, J.S. 1990 Liquid metal flow through a sharp elbow in the plane of a strong magnetic field, *J. Fluid Mech.*, vol. 213, 273–292

Moon, T.J. & Hua, T.Q. &Walker, J.S. 1990 Liquid metal flow in a backward elbow in the plane of a strong magnetic field, *J. Fluid Mech.*, vol. 227, 373–292.

Smith,D.L. *et al.* 1985 Blanket comparison and selection study. *Fusion Technolgy. **8**, 1.*

Walker, J.S. 1981 Magnetohydrodynamic flows in rectangular ducts with thin conducting walls, *Journal de Mécanique*, vol. 20, No.1, 79.